Progress In Electromagnetics Research M, Vol. 111, 235–246, 2022

Design of a Microstrip Sensor Based on a CSRR-Derived Structure for Measuring the Permittivity and Permeability of Materials

Yun-Rui Wang* **and Hong-Gang Hao**

Abstract—In this paper, a microstrip sensor based on a complementary split ring resonator (CSRR)-derived structure is proposed to characterize the permittivity and permeability of materials. By loading an etched meandered conductive ring and an interdigital capacitor structure, effective separation of the permittivity sensing area and permeability sensing area is realized, and the field strengths of the corresponding areas are improved. The relationship between the resonant response (resonant frequency and quality factor) of the sensor and the permittivity and permeability of the sample under test (SUT) is discussed, and the theoretical basis for measuring the material properties is given. By analyzing the measured resonant frequency and quality factor, the real and imaginary parts of the permittivity and permeability of the SUT can be determined. The sensor was fabricated on a Rogers 5880 substrate, and four standard dielectric and magnetodielectric (MD) samples were tested. The results show that the measured values of the real and imaginary parts of the permittivity and permeability are in good agreement with the reference data.

1. INTRODUCTION

Accurate measurement of the permittivity and permeability of magnetodielectric (MD) materials plays an important role in the food industry, agriculture, medical and health care, military and national defense, and other fields. At present, the methods for measuring the material properties can be classified as the transmission line method [1], free space method [2], waveguide method [3], and microwave resonant method [4, 5]. The transmission line method has low sensitivity, but the operation is simple, and the permittivity and permeability can be measured over a wide frequency band. The free space method can measure a wide frequency range, but the system design is complex. The waveguide method has high requirements for sample preparation. It can measure the properties of thinner samples and has high measurement accuracy.

The microwave resonant method can produce strong magnetic and electric fields on the surface of a resonant structure. When the sample under test (SUT) is placed on the surface as a perturbation, resonance characteristics such as resonant frequency and quality factor are affected. Therefore, the material properties can be extracted from the changes in the resonance characteristics after the SUT is placed. Compared with the other methods, the microwave resonant method has the advantages of being a simple and low-cost method while maintaining the sensitivity and accuracy [6].

The application of basic resonant elements such as split ring resonators (SRRs) and complementary split ring resonators (CSRRs) improves the performance of previous microwave sensors. It not only improves the accuracy and sensitivity of measurement but also simplifies the measurement steps. Muhammed Shafi et al. proposed an interdigital capacitor-based split ring resonator (IDC-SRR) and a meandered line-based split ring resonator (ML-SRR). They can be used to measure the permittivity

Received 25 May 2022, Accepted 17 June 2022, Scheduled 19 July 2022
* Corresponding author: Yun-Rui Wang (645820206@qq.com).
The authors are with the College of Electronic Engineering, Chongqing University of Posts and Telecommunications, Chongqing 400065, China.

and permeability of materials. They work at a 2.45 GHz frequency and have high sensitivity, with a measurement error of less than 6% [7]. However, the permittivity and permeability of the SUT need to be measured by two different resonators, which increases the cost and complicates the characterization process. In the same year, the previous team proposed a new SRR microwave resonator for measuring the properties of MD materials. These materials cause the resonator to produce two different resonant frequencies. The two resonant frequencies can characterize the real part of the permittivity and permeability of the SUT [8]. However, due to the interference between permittivity and permeability measurements, the measurement error is 8%. Reference [9] used a CSRR-derived structure to design a resonator that can measure the real and imaginary parts of the permittivity and permeability by locating the strongest electric field and magnetic field in different regions. It operates at a frequency of 2.47 GHz, with a maximum error of 1.81%. However, the sensor has high cross-interference and poor electromagnetic separation characteristics. The different permittivity and permeability sensing areas lead to the preparation of different size samples. A planar microwave sensor for characterizing the permittivity and permeability of MD media was proposed in [10]. The SUTs were placed in the permittivity and permeability sensing areas of the sensor to characterize the properties of the material, with a relative error of less than 5%. However, there will be unavoidable mutual interference in the measurement of parameters due to the coupling between two CSRR structures.

To avoid the complex and cumbersome process of parameter extraction in the measurement of multiple devices or the mutual interference of the electric field and magnetic field in the measurement of a single device at the same time, in this paper, a permittivity and permeability microstrip sensor based on the [7] CSRR-derived structure is proposed. Contrary to the effect that the meandered conductive ring and interdigital capacitor structure described in [7] can achieve aggregation of the magnetic field and electric field, this paper etches these two structures on a metal ground to achieve the effect complementary to that in [7], i.e., the curved meandered conductive ring and interdigital capacitor can achieve aggregation of the electric field and magnetic field, respectively. This makes the electric field and magnetic field concentrated in different areas of the sensor for characterization of the electrical and magnetic parameters of the SUT, respectively. At the same time, it significantly improves the strength of the fields in the sensing areas. In general, the sensor has a simple structure and low cost and can satisfy the electrical and magnetic properties of single device characterization materials.

2. SENSOR STRUCTURE AND WORKING PRINCIPLE

According to perturbation theory, when the SUT is placed on the surface or inside a microwave resonator, the existence of the sample disturbs the original electric and magnetic field distributions, resulting in changes in the frequency and quality factor of the resonator, reducing the Q-value, and moving the resonant frequency to low frequency [9]. The relationship between the change in the resonant frequency and the properties of the material can be specifically expressed as follows:

$$\frac{\Delta f_r}{f_r} = \frac{\int_{vs} \Delta\varepsilon \mathbf{E}_1 \cdot \mathbf{E}_0 + \Delta\mu \mathbf{H}_1 \cdot \mathbf{H}_0}{\int_v \varepsilon_0 |\mathbf{E}_0|^2 + \mu_0 |\mathbf{H}_0|^2} \tag{1}$$

where Δf_r is the frequency change of the resonator after SUT placement, and f_r is the initial frequency of the resonator. vs is the perturbation volume; v is the volume of the electromagnetic field that exists in space; ε_0 and μ_0 are the permittivity and permeability of vacuum; $\mathbf{E}_0$, $\mathbf{H}_0$, $\mathbf{E}_1$, and $\mathbf{H}_1$ are the electric field and magnetic field of the resonator before and after placing the SUT; and $\Delta\varepsilon$ and $\Delta\mu$ are the changes in the permittivity and permeability. Compared with other parts of the resonator, the perturbation material has little effect, and as an approximation, $\mathbf{E}_1 = \mathbf{E}_0$, and $\mathbf{H}_1 = \mathbf{H}_0$; thus, (1) can be changed to

$$\frac{\Delta f_r}{f_r} = \frac{\int_{vs} \Delta\varepsilon |\mathbf{E}_0|^2 + \Delta\mu |\mathbf{H}_0|^2}{\int_v \varepsilon_0 |\mathbf{E}_0|^2 + \mu_0 |\mathbf{H}_0|^2} \tag{2}$$

According to (2), if the electric field has high intensity, and the magnetic field strength is very low ($\mathbf{H}_0 \approx 0$) in the resonant volume, then a change in the permittivity of the SUT has a greater influence on the resonant frequency, and a change in the permeability has little effect on the resonant frequency. Similarly, if the magnetic field has high intensity and the electric field intensity is very low ($\mathbf{E}_0 \approx 0$), then a change in the permeability of the SUT has a greater influence on the resonant frequency, and a change in the permittivity has little effect on the resonant frequency.

As mentioned above, by designing the structure of the sensor, the strong magnetic field area and strong electric field area in the sensor are distributed at different positions of the sensor. The electric permittivity of the SUT is tested by loading it in the region where the electric field intensity is very strong, and the magnetic field intensity is almost zero. In contrast, the magnetic permeability of the SUT is tested by loading it in the region where the magnetic field intensity is very strong, and the electric field intensity is almost zero. Therefore, a single resonator can be used to determine the permittivity and permeability.

Figure 1 shows the perspective view of the proposed sensor. A Rogers 5880 laminate with a dielectric constant of 2.2, a loss tangent of 0.0009, and a thickness of 0.787 mm is used as the substrate. The metal layer thickness is 0.035 mm, and the width of the microstrip line is set to 2.35 mm to provide a characteristic impedance of 50 Ω. The bottom layer of the sensor is a derived structure of the CSRR, which is composed of an etched meandered conductive ring and an interdigital capacitor, and the top layer is a microstrip.

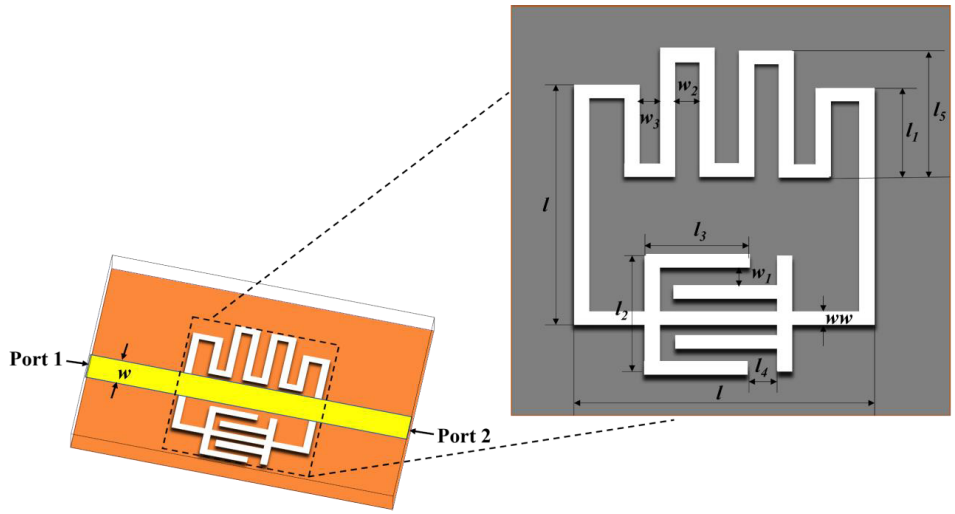

Figure 1. Perspective view of the proposed sensor. The dimensions of the sensor are: $l = 6.6$ mm, $l_1 = 1.6$ mm, $l_2 = 3.6$ mm, $l_3 = 1.9$ mm, $l_4 = 0.3$ mm, $l_5 = 2.6$ mm, $w_1 = 0.4$ mm, $w_2 = 0.4$ mm, $w_3 = 0.4$ mm, $ww = 0.4$ mm, $w = 2.35$ mm.

The equivalent circuit of the proposed microstrip sensor is shown in Fig. 2, and its resonant frequency can be expressed as [11]

$$f_r = \frac{1}{2\pi\sqrt{L_r(C_c + C_r)}} \tag{3}$$

where C_r and L_r are the equivalent capacitance and inductance of the etched ring with a width of ww; C_c represents the coupling capacitance between the microstrip line and the etched ring; and L is the line inductance.

The frequency response of the sensor is shown in Fig. 3. The proposed sensor exhibits a resonant frequency of 2.40 GHz and a quality factor of 148.

The permittivity sensing area needs to meet the requirements that the electric field intensity is high, and the magnetic field intensity is very low ($\mathbf{H} \approx 0$). The permeability sensing area needs to meet the requirements that the magnetic field intensity is high, and the electric field intensity is very low ($\mathbf{E} \approx 0$). When the two sensing areas can be clearly separated, the interference between the

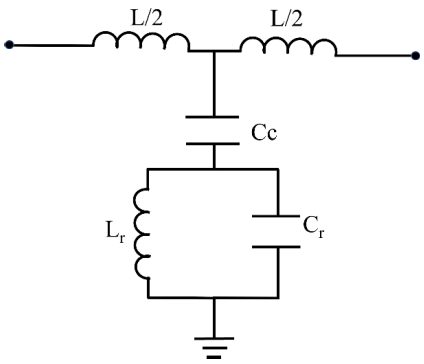

Figure 2. Equivalent circuit model of the proposed electromagnetic parameter sensor. The electrical parameters are $C_r = 1.62\,\text{pF}$, $L_r = 1.68\,\text{nH}$, $C_c = 0.15\,\text{pF}$, and $L = 1.48\,\text{pF}$.

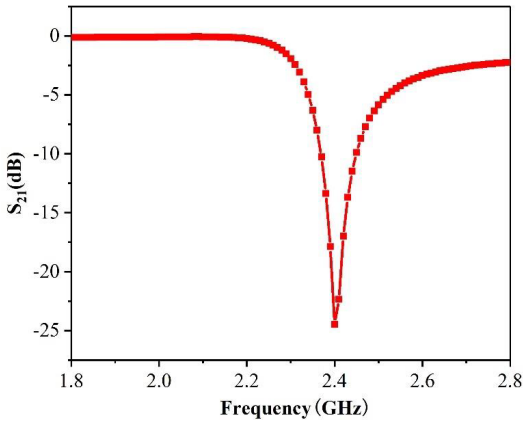

Figure 3. Frequency response of the proposed sensor.

permittivity and permeability of the SUT can be minimized when being measured separately. The **E** and **H** distributions on the metal ground plane at the resonant frequency are depicted in Figs. 4(a) and (b), respectively.

In the permittivity sensing area in Fig. 4(a), the electric field intensity reaches the maximum, and

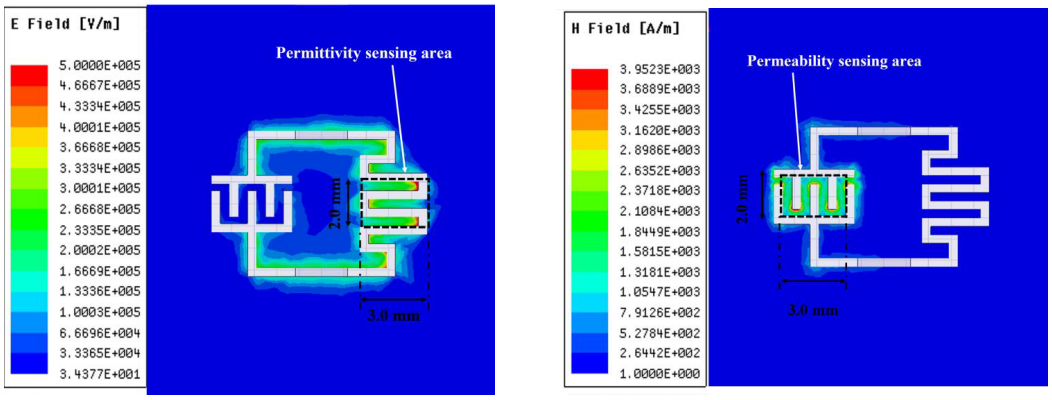

(a) (b)

Figure 4. Magnitudes of the (a) electric and (b) magnetic field distributions on the ground plane at the resonant frequency.

the magnetic field almost disappears. Therefore, when a fixed size SUT is placed in this area, the changes in the resonant frequency and notch magnitude of the sensor are only induced by the permittivity of the SUT, and the influence of the permeability of the SUT can be ignored. In the permeability sensing area in Fig. 4(b), the magnetic field reaches the maximum, and the electric field is almost zero. Similarly, by placing an SUT of fixed size in this area, its permeability can be accurately measured. These two regions can be concluded to be the best areas to detect changes in the permittivity and permeability of the SUT.

3. SIMULATION AND ANALYSIS

According to [12] under microwave conditions, the variation ranges of ε_r and $\tan\delta_e$ of MD materials in a real environment are $1 \sim 10$ and $0 \sim 0.1$, while the variation ranges of μ_r and $\tan\delta_m$ are $1 \sim 2$ and $0 \sim 0.5$. Here, the steps are set as 1, 0.02, 0.2, and 0.1. To obtain more accurate results, a 15 µm air gap between the SUT and the sensor metal ground is considered in the simulation. In addition, the thickness of the sample will also affect the response of the sensor. Since the field is highly localized near the CSRR-derived structure, when the thickness of the SUT reaches a certain value, the interaction of the field with the SUT saturates, which makes the sensor response change little. According to the simulation results, to minimize the influence of sample thickness, the thickness of the SUT is set to 0.5 mm in this paper.

According to the above analysis, for the permeability measurement the SUT needs to be placed in the area where the magnetic field intensity is high, and the electric field intensity is very low ($\mathbf{E} \approx 0$). To verify that the resonant response in the permeability sensing region is caused only by the change in the permeability of the SUT and is unrelated to the change in the permittivity, ε_r and $\tan\delta_e$ of the SUT are changed in the permeability sensing region while keeping $\mu_r = 1$ and $\tan\delta_m = 0$. The response results of the sensor are shown in Fig. 5.

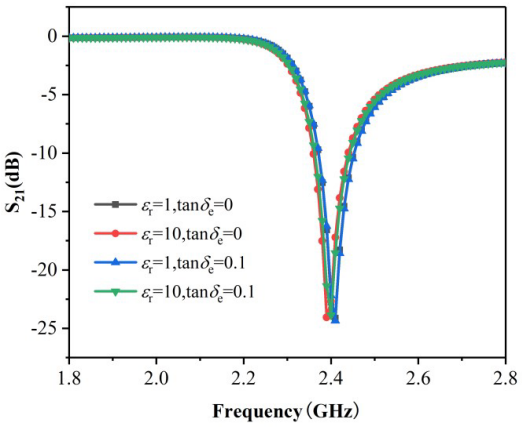

Figure 5. Sensor response for different complex permittivities of the SUT when the sample is placed in the permeability sensing area.

As shown in Fig. 5, since the electric field intensity in the permeability sensing area is very low, the changes in ε_r and $\tan\delta_e$ have no obvious effect on the resonant frequency and quality factor. The response of the sensor is only related to the permeability of the SUT and is unrelated to the permittivity of the SUT.

Figures 6(a) and (b) show S_{21} for different values of μ_r and $\tan\delta m$ when $\tan\delta_m = 0$ and $\mu_r = 1$, respectively. When μ_r changes from 1 to 2, the resonant frequency changes from 2.41 GHz to 2.23 GHz; the offset of the resonant frequency is 0.18 GHz; and the notch magnitude is maintained at approximately -25 dB. In contrast, the change in $\tan\delta_m$ has little effect on the offset of the resonant frequency, and the resonant frequency is maintained at approximately 2.41 GHz. Therefore, the change in the resonant frequency can be used to accurately measure the μ_r of the SUT.

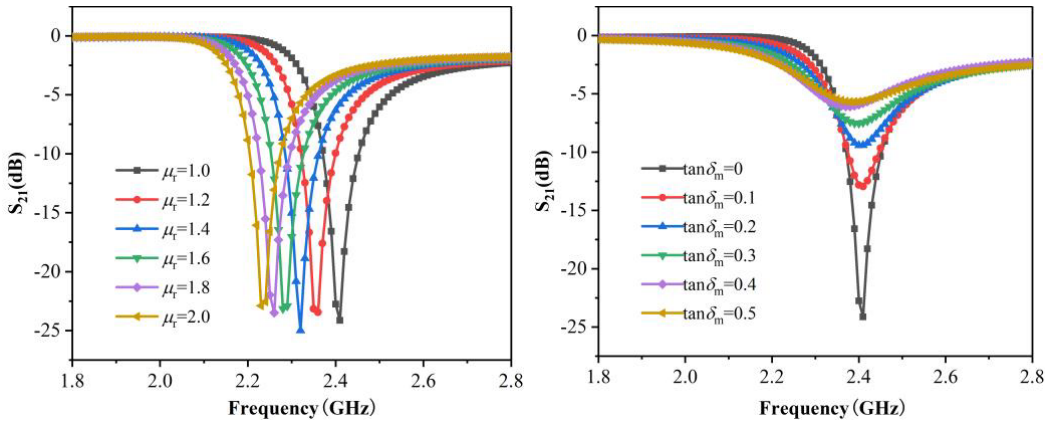

Figure 6. Sensor response for different (a) μ_r ($\tan\delta_m = 0$) and (b) $\tan\delta_m$ ($\mu_r = 1$) when the SUT is placed in the permeability sensing area.

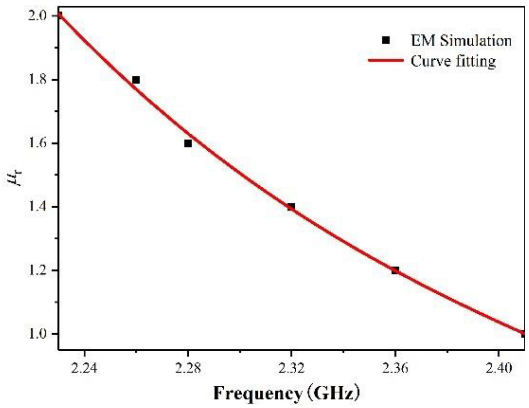

Figure 7. Permeability (μ_r) of the SUT as a function of the resonant frequency.

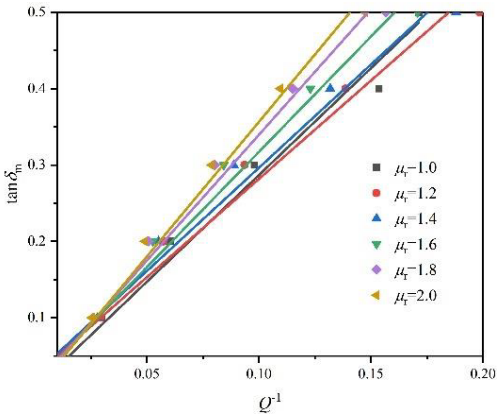

Figure 8. Magnetic loss tangent ($\tan\delta_m$) against the inverse quality factor for different values of $\mu_r = 1, 1.2, 1.4, 1.6, 1.8, 2$.

Figure 7 shows the fitting of the resonant frequency and permeability of the SUT by using curve fitting technology. The resonant frequency shifts to a low frequency with increasing μ_r of the SUT, and μ_r as a function of the resonant frequency f_r is given as

$$\mu_r = 462.358 - 553.641 f_r + 222.653 f_r^2 - 30.025 f_r^3 \tag{4}$$

Figure 6(b) shows that when μ_r is fixed, with increasing magnetic loss tangent $\tan\delta_m$, the notch magnitude and quality factor of the S_{21} curve decrease. Here, the quality factor can be used to characterize the magnetic loss tangent, which can be defined as $Q = f_r/\Delta f$, where f_r is the resonant frequency, and Δf is the 3-dB bandwidth. Fig. 8 shows the relationship between the magnetic loss tangent $\tan\delta_m$ and the inverse quality factor Q^{-1} at different values of μ_r. As $\tan\delta_m$ changes from 0 to 0.5, Q significantly decreases, and Q^{-1} changes from 0.01 to 0.20. The fitting function is as follows:

$$\tan\delta_m = (3.911 + 3805Q^{-1} - 48.99\mu_r - 8798Q^{-2} + 500.5Q^{-1}\mu_r + 18.26\mu_r^2) \times 10^{-3} \tag{5}$$

Similarly, to characterize the dielectric properties of the SUT, it needs to be placed in the permittivity sensing region, where the electric field intensity is high, and the magnetic field intensity is very low ($\mathbf{H} \approx 0$). Likewise, to verify that the resonant response in the permittivity sensing region is only due to the change in the permittivity of the sample and is independent of the change in the permeability, the response of the sensor is observed by placing the SUT in the permittivity sensing area

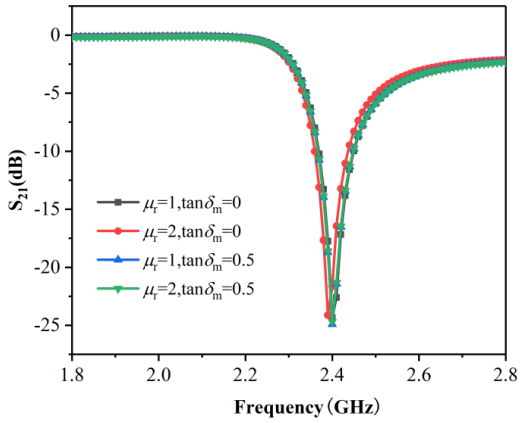

Figure 9. Sensor response for different complex permeabilities of the SUT when the sample is placed in the permittivity sensing area.

and changing its μ_r and $\tan\delta_m$ while keeping $\varepsilon_r = 1$ and $\tan\delta_e = 0$. The results are shown in Fig. 9. Due to the extremely low magnetic field strength in the permittivity sensing region, the changes in μ_r and $\tan\delta_m$ have no significant effect on the resonant frequency and quality factor. The response of the sensor is only related to the permittivity of the SUT and is unrelated to the permeability of the SUT.

Figures 10(a) and (b) show S_{21} for different values of ε_r and $\tan\delta_e$ when $\tan\delta_e = 0$ and $\varepsilon_r = 1$, respectively. As ε_r increases from 1 to 10, the resonant frequency of the resonator decreases from 2.40 GHz to 2.09 GHz, and the offset of the resonant frequency is 0.31 GHz. In contrast, the change in $\tan\delta_e$ does not cause a resonant frequency shift, and the resonant frequency is maintained at approximately 2.40 GHz. Therefore, the change in the resonant frequency can be used to accurately measure the SUT ε_r.

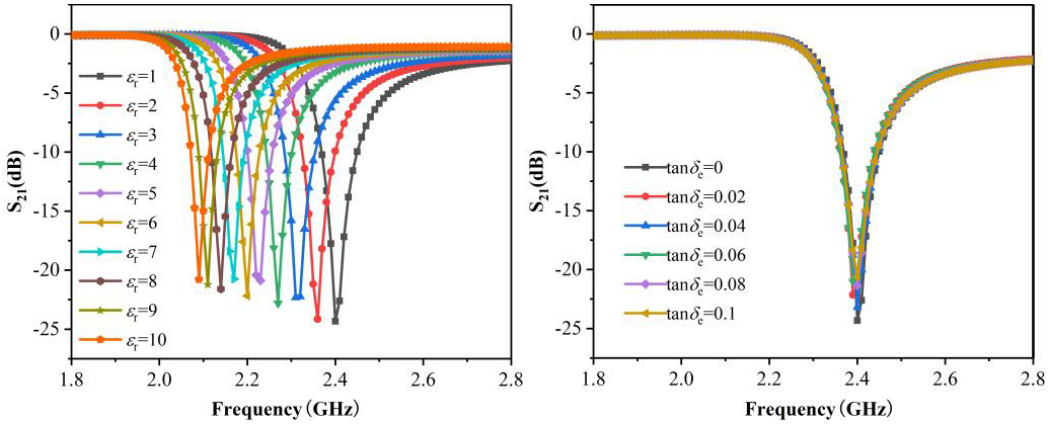

Figure 10. Sensor response for different (a) ε_r ($\tan\delta_e = 0$) and (b) $\tan\delta_e$ ($\varepsilon_r = 1$) when the SUT is placed in the permittivity sensing area.

Figure 11 shows the fitting between the resonant frequency and the permittivity of the SUT. The resonant frequency shifts to a low frequency with increasing ε_r of the SUT, and ε_r as a function of the resonant frequency f_r is given as

$$\varepsilon_r = 1019.04 - 1224.226 f_r + 498.881 f_r^2 - 68.9697 f_r^3 \tag{6}$$

Figure 12 shows the relationship between the electric loss tangent $\tan\delta_e$ and the inverse quality factor Q^{-1} at different values of ε_r. As $\tan\delta_e$ changes from 0 to 0.1, Q significantly decreases, and Q^{-1}

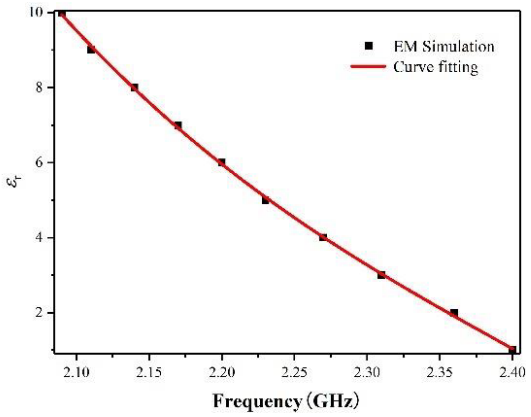

Figure 11. Permittivity (ε_r) of the SUT as a function of the resonant frequency.

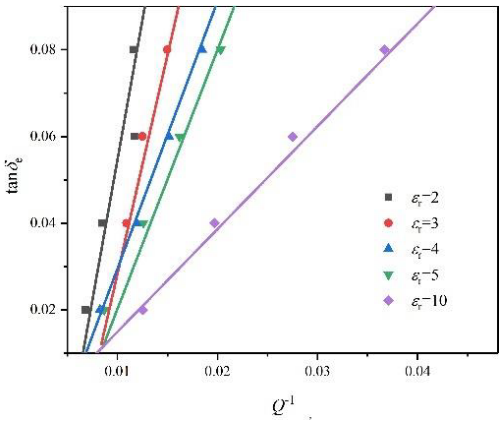

Figure 12. Electric loss tangent ($\tan\delta_e$) against the inverse quality factor for different values of $\varepsilon_r = 2, 3, 4, 5, 10$.

changes from 0.01 to 0.05. The fitting function is as follows:

$$\tan\delta_e = (-2.634 + 1136Q^{-1} - 1.261\varepsilon_r - 1085Q^{-2} - 85.16Q^{-1}\varepsilon_r + 0.1411\varepsilon_r^2) \times 10^{-2} \tag{7}$$

4. MEASUREMENT AND RESULTS

Based on the microstrip sensor with the CSRR-derived structure in Fig. 1, a real measurement device was fabricated, as shown in Fig. 13. An Agilent vector network analyzer N5242A was used to measure the S parameters. Four kinds of standard plates, Rogers RO4350, FR4, Fe_3O_4-PDMS (30%), and Fe_3O_4-PDMS (50%), were used as test samples. Note that the samples must be precisely cut to the specified size and prepared according to the dimensions of 2.0 mm × 3.0 mm × 0.5 mm. In the actual measurement, the sample is fixed and accurately placed according to the corresponding positions of the permittivity and permeability sensing regions in Fig. 4 to reduce the interference caused by the measurement process.

To verify the correctness of the simulation, Fig. 14 depicts the simulated and measured S_{21} values of the sensor when different samples are loaded in different sensing areas. This figure shows that the simulated and measured S_{21} values have strong consistency and are in good agreement.

Figures 15(a) and (b) show the measured S_{21} of the sensor when different samples are loaded in the permittivity and permeability sensing area. The resonant frequency and quality factor are extracted from S_{21}. The complex permittivity (ε_r and $\tan\delta_e$) and complex permeability (μ_r and $\tan\delta_m$) can be obtained according to the characterization expressions (4), (5), (6), and (7) given in Section 3.

The values of ε_r, $\tan\delta_e$, μ_r, and $\tan\delta_m$ are provided in Table 1. By comparing the data in Table 1, the values of the permittivity and permeability of the four samples measured by the proposed sensor can be seen basically in agreement with the nominal values given in [13, 14], and the accuracy is high.

The etched meandered conductive ring and interdigital capacitor structure in the sensor can effectively separate the permittivity sensing area and the magnetic sensing area and reduce the problems caused by the mutual interference between electric and magnetic fields during parameter measurement. At the same time, the electric field strength in the permittivity sensing area and the magnetic field strength in the permeability sensing area are significantly improved, thereby improving the measurement sensitivity. Table 2 shows some parameter comparisons with related literature [7, 9, 10, 14]. The proposed sensor is capable of exhibiting a performance comparable to that of the previous designs, where S_{fm} and S_{fe} are the sensitivities at μ_r and ε_r, respectively, which can be separately defined as

$$S_{fm} = \frac{f_{r\_u} - f_{r\_sut}}{f_{r\_u}} \cdot \frac{1}{\mu_r - 1} \tag{8}$$

$$S_{fe} = \frac{f_{r\_u} - f_{r\_sut}}{f_{r\_u}} \cdot \frac{1}{\varepsilon_r - 1} \tag{9}$$

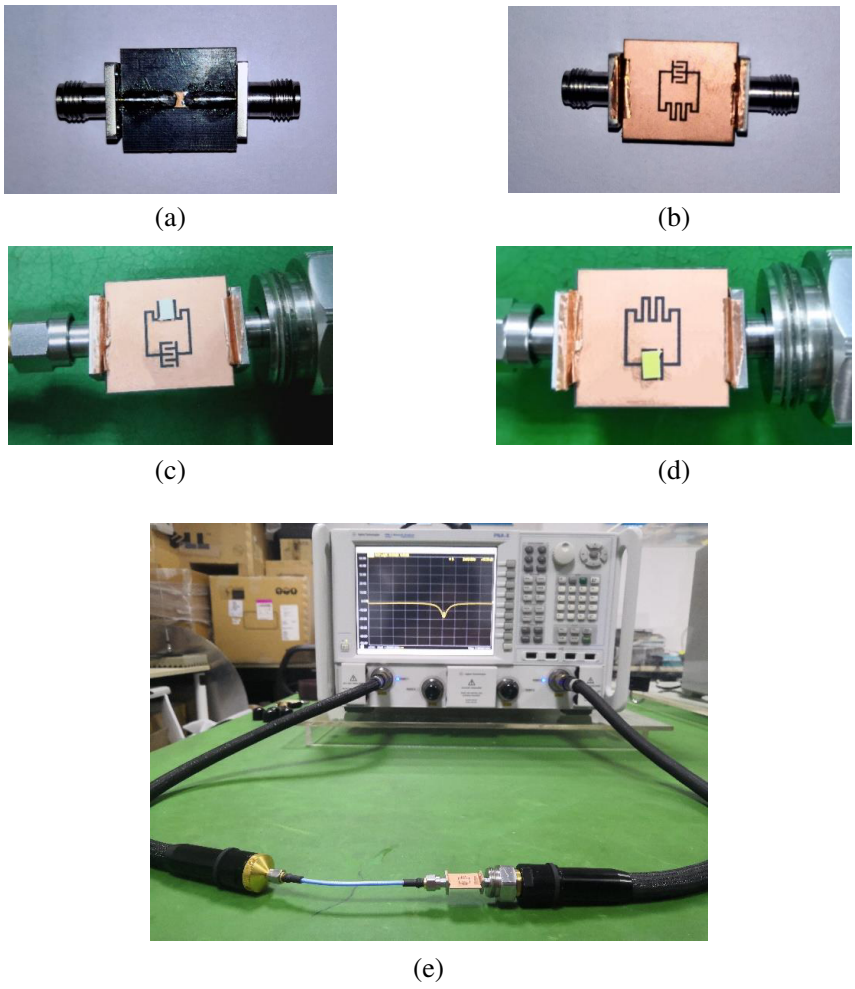

Figure 13. Fabricated prototype of the proposed sensor: (a) Top view of the proposed sensor. (b) Bottom view of the proposed sensor. (c) Permittivity sensing area. (d) Permeability sensing area. (e) Experimental setup.

Table 1. Measured complex permittivity and permeability for SUT materials.

SUT	ε_r		$\tan\delta_e$		μ_r		$\tan\delta_m$	
	This Work	Reference	This Work	Reference	This Work	Reference	This Work	Reference
FR4 [14]	4.31	4.4	0.042	0.02	1	1	0	0
Rogers4350 [14]	3.52	3.48	0	0.004	1	1	0	0
Fe_3O_4(30%) [13]	2.79	2.81	0.073	0.075	1.26	1.25	0.048	0.05
Fe_3O_4(50%) [13]	2.68	2.7	0.163	0.120	1.51	1.49	0.082	0.09

where f_{r_u} and f_{r_sut} are the resonant frequencies of the sensor when the sensor has no load and when the corresponding load is loaded, respectively.

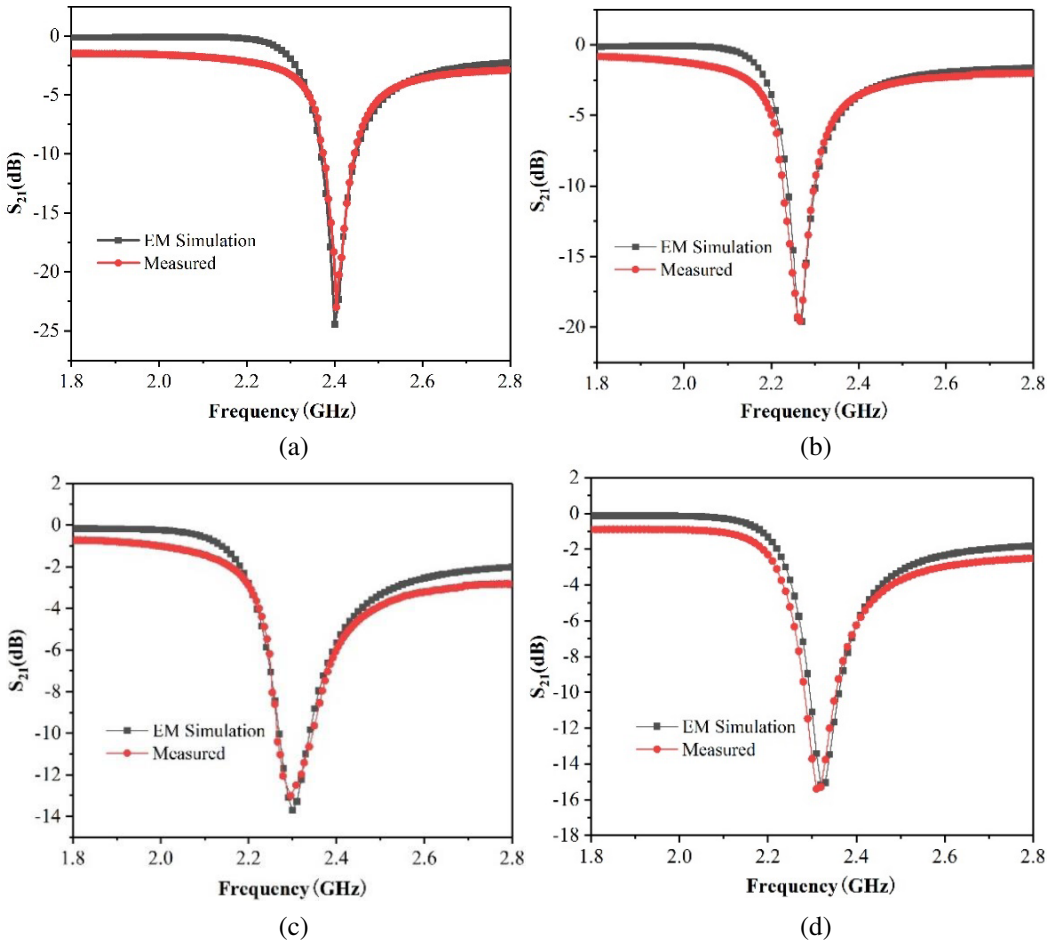

Figure 14. Comparison between the simulated and measured S_{21} of (a) the unloaded sensor, (b) the sensor loaded with FR4 in the permittivity sensing area, (c) the sensor loaded with Fe_3O_4-PDMS (50%) in the permeability sensing area, and (d) the sensor loaded with Fe_3O_4-PDMS (50%) in the permittivity sensing area.

Table 2. Measured complex permittivity and permeability for SUT materials.

	[7]	[9]	[10]	[14]	Proposed
f_u (GHz)	2.45	2.47	2.24	2.22	2.40
Q	260	145	1119	267/653	148
S_{fm} ($\times 10^{-2}$)	3.89	6.86	$\sim$ 3.35	-	7.47
S_{fe} ($\times 10^{-2}$)	4.78	2.40	$\sim$ 1.39	1.85/1.72	1.44
Number of measured parameters	2	4	2	1	4

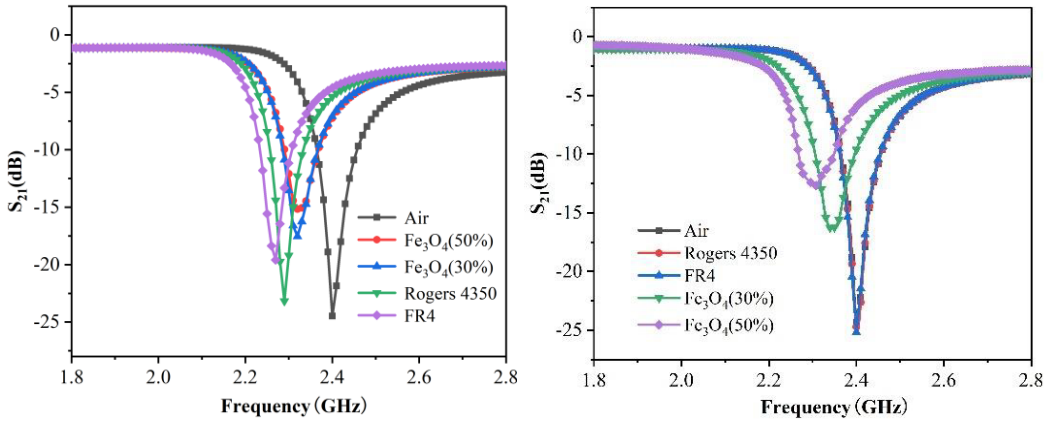

Figure 15. Measured S_{21} of the sensor when different samples are loaded in (a) the permittivity sensing area and (b) in the permeability sensing area.

5. CONCLUSION

A microstrip sensor with a CSRR-derived structure is proposed in this paper, which can realize a single device to characterize the real and imaginary parts of the permittivity and permeability of a SUT. The meandered conductive ring and interdigital capacitor etched on the metal ground allow the electric and magnetic fields to be concentrated in different areas of the sensor and significantly increase the field strength in the sensing area. The area with a strong magnetic field but a weak electric field is used as the permeability sensing area, and the area with a strong electric field but a weak magnetic field is used as the permittivity sensing area. ε_r, $\tan\delta_e$, μ_r, and $\tan\delta_m$ of the SUT were determined by placing the SUT in the corresponding sensing area and analyzing the changes in the resonant frequency and quality factor. Finally, various SUTs were fabricated, and the electrical and magnetic parameters were measured by using the proposed sensor and applying the characterization procedure presented in this paper. The measured values agree well with the reference values, which verifies the validity of the sensor.

REFERENCES

1. Takach, A. A., F. M. Mbango, F. Ndagijimana, M. Al-Husseini, and J. Jomaah, "Two-line technique for dielectric material characterization with application in 3D-printing filament electrical parameters extraction," *Progress In Electromagnetics Research M*, Vol. 85, 195–207, 2019.
2. Naik, S., M. Pour, and C. Hill, "Characterization of dielectric properties of non-magnetic materials using superstrate-loaded antennas," *Progress In Electromagnetics Research M*, Vol. 104, 39–47, 2021.
3. Benali, L. A., J. Terhzaz, A. Tribak, and A. M. Sanchez, "2D-FDTD method to estimate the complex permittivity of a multilayer dielectric materials at Ku-band frequencies," *Progress In Electromagnetics Research M*, Vol. 91, 155–164, 2020.
4. Hao, H., D. Wang, and W. Zhu, "A permittivity measurement method based on back propagation neural network by microwave resonator," *Progress In Electromagnetics Research C*, Vol. 110, 27–38, 2021.
5. Karami, M., P. Rezaei, S. Kiani, and R. A. Sadeghzadeh, "Modified planar sensor for measuring dielectric constant of liquid materials," *Electronics Letters*, Vol. 53, No. 19, 1300–1302, Sept. 2017.
6. Ansari, M. A. H., A. K. Jha, Z. Akhter, and M. J. Akhtar, "Multi-band RF planar sensor using complementary split ring resonator for testing of dielectric materials," *IEEE Sensors J.*, Vol. 18, 6596–6606, Aug. 16, 2018.

7. Muhammed Shafi, K. T., A. K. Jha, and M. J. Akhtar, "Improved planar resonant RF sensor for retrieval of permittivity and permeability of materials," *IEEE Sensors J.*, Vol. 17, No. 17, 5479–5486, Sept. 2017.
8. Muhammed Shafi, K. T., M. A. H. Ansari, A. K. Jha, and M. J. Akhtar, "Design of SRR-based microwave sensor for characterization of magnetodielectric substrates," *IEEE Microw. Wirel. Components Lett.*, Vol. 27, No. 5, 524–526, May 2017.
9. Saadat-Safa, M., V. Nayyeri, M. Khanjarian, M. Soleimani, and O. M. Ramahi, "A CSRR-based sensor for full characterization of magneto-dielectric materials," *IEEE Trans. Microw. Theory Tech.*, Vol. 67, No. 2, 806–814, Feb. 2019.
10. Gan, H.-Y., et al., "A CSRR-loaded planar sensor for simultaneously measuring permittivity and permeability," *IEEE Microw. Wirel. Components Lett.*, Vol. 30, No. 2, 219–221, Feb. 2020.
11. Bonache, J., M. Gil, I. Gil, J. Garcia-Garcia, and F. Martin, "On the electrical characteristics of complementary metamaterial resonators," *IEEE Microw. Wirel. Components Lett.*, Vol. 16, No. 10, 543–545, Sept. 2006.
12. Gama, A. M. and M. C. Rezende, "Complex permeability and permittivity variation of carbonyl iron rubber in the frequency range of 2 to 18 GHz," *J. Aerosp. Technol. Manage.*, Vol. 2, No. 1, 59–62, Apr. 2010.
13. Castro, J., C. Morales, T. Weller, et al., "Synthesis and characterization of low-loss Fe_3O_4-PDMS magneto-dielectric polymer nanocomposit," *15th IEEE Annual Conference on Wireless and Microwave Technology (WAMICON)*, 1–5, Tampa, FL, USA, 2014.
14. Alahnomi, R. A., Z. Zakaria, E. Ruslan, S. R. Ab Rashid, and A. A. Mohd Bahar, "High-Q sensor based on symmetrical split ring resonator with spurlines for solids material detection," *IEEE Sensors J.*, Vol. 17, No. 9, 2766–2775, May 2017.